remote sensing

MDPI

Article

Urban Morphology and Surface Urban Heat Island Relationship During Heat Waves: A Study of Milan and Lecce (Italy)

Antonio Esposito [1], Gianluca Pappaccogli [1,*], Antonio Donateo [2], Pietro Salizzoni [3], Giuseppe Maffeis [4], Teodoro Semeraro [5], Jose Luis Santiago [6] and Riccardo Buccolieri [1,2]

[1] Department of Biological and Environmental Sciences and Technologies, University of Salento, S.P. 6 Lecce-Monteroni, 73100 Lecce, Italy; antonio.esposito@unisalento.it (A.E.); riccardo.buccolieri@unisalento.it (R.B.)
[2] Institute of Atmospheric Sciences and Climate (ISAC), National Research Council (CNR), Str. prov. Lecce-Monteroni, Km 1,2, 73100 Lecce, Italy; a.donateo@isac.cnr.it
[3] Laboratoire de Mécanique des Fluides et d'Acoustique, University of Lyon, CNRS UMR 5509, Ecole Centrale de Lyon, INSA Lyon, Université Claude Bernard, 36, Avenue Guy de Collongue, 69134 Ecully, France; pietro.salizzoni@ec-lyon.fr
[4] TerrAria s.r.l., Via Melchiorre Gioia 132, 20125 Milan, Italy; g.maffeis@terraria.com
[5] Research Institute on Terrestrial Ecosystems (IRET-URT Lecce), National Research Council of Italy (CNR), Campus Ecotekne, 73100 Lecce, Italy; teodoro.semeraro@cnr.it
[6] Atmospheric Modelling Unit, Environmental Department, CIEMAT, 28040 Madrid, Spain; jl.santiago@ciemat.es
* Correspondence: gianluca.pappaccogli@unisalento.it

Abstract: The urban heat island (UHI) effect, marked by higher temperatures in urban areas compared to rural ones, is a key indicator of human-driven environmental changes. This study aims to identify the key morphological parameters that primarily contribute to the development of surface urban heat island intensity (SUHII) and investigates the relationship between SUHII and urban morphology using land surface temperature (LST) data from the Sentinel-3 satellite. The research focuses on Milan and Lecce, analyzing how urban geometry affects SUHII. Factors such as building height, aspect ratio, sky visibility, and surface cover are examined using approximately 1000 satellite images from 2022 and 2023. The study highlights seasonal and diurnal variations in SUHII, with particular emphasis on HW periods. Through multicollinearity and multiple regression analyses, the study identifies the main morphological drivers influencing SUHII in the two cities, specifically the Impervious Surface Fraction (ISF) and Mean Building Height (HM). Milan consistently exhibits higher SUHII, particularly during HWs, while Lecce experiences a negative SUHII, especially during the summer, due to lower urban density, more vegetation, and the low soil moisture around the urban area. Both cities show positive SUHII values at night, which are slightly elevated during HWs. The heat wave analysis reveals the areas most susceptible to overheating, typically characterized by high urban density, with ISF and HM values in some cases above the 90th percentile (0.8 and 13.0 m, respectively) compared to the overall distribution, particularly for Milan. The research emphasizes the importance of urban morphology in influencing SUHII, suggesting that detailed morphological analysis is crucial for developing climate adaptation and urban planning strategies to reduce urban overheating and improve urban resilience to climate change.

Keywords: SUHII; Sentinel-3 satellite; urban morphological parameters; heat waves; cool island effect

Citation: Esposito, A.; Pappaccogli, G.; Donateo, A.; Salizzoni, P.; Maffeis, G.; Semeraro, T.; Santiago, J.L.; Buccolieri, R. Urban Morphology and Surface Urban Heat Island Relationship During Heat Waves: A Study of Milan and Lecce (Italy). *Remote Sens.* **2024**, *16*, 4496. https://doi.org/10.3390/rs16234496

Academic Editors: Christiane Weber and Jingxia Wang

Received: 19 September 2024
Revised: 27 November 2024
Accepted: 27 November 2024
Published: 30 November 2024

1. Introduction

The urban influence on local microclimates, particularly through the urban heat island (UHI) effect, is one of the most important factors in human-induced environmental changes, as cities experience higher temperatures than surrounding rural areas [1]. The main elements influencing urban climate include the thermal and radiative properties of urban materials and structures, such as high aspect ratios (the ratio of building height to

street width) and a high impervious surface fraction (ISF). These factors lead to multiple reflections of solar and infrared radiation, resulting in heat accumulation during the day and a gradual release at night, maintaining a positive sensible heat flux which is trapped within the street volumes [2,3]. Additionally, the low pervious surface fraction (PSF) in cities reduces latent heat flux and cooling by evapotranspiration [4]. Likewise, anthropogenic heat from human activities contributes an additional component to the surface energy balance [5]. The study of urban climate employs different but complementary methods, each offering its own advantages depending on the objective pursued [1]. In situ data from permanent weather stations continuously measure key weather parameters but typically have limited spatial coverage [6]. In contrast, remotely sensed thermal infrared data offer a simultaneous view of entire urban areas, but lack adequate temporal resolution, which often fails to investigate surface thermal dynamics through daily cycles [6].

In recent decades, remote sensing bridged this gap, making available products with high spatial and temporal resolutions. Global land surface temperature (LST) observations have been accessible through satellite observations in the thermal infrared, with spatial resolutions of less than 2 km. Long-term operational satellites like MODIS (MOD11) have provided valuable data for over a decade (https://modis.gsfc.nasa.gov/data/dataprod/mod11.php, accessed on 18 September 2024). Recently, new large-scale satellite LST products have emerged, including those from Sentinel-3, which captures global land and sea surface temperatures using three thermal infrared bands. Recent analyses in European cities, exemplified by the work of Agathangelidis et al. [7] using MODIS LST data, have shown significant correlations between surface temperature and several urban morphological parameters, whereas factors such as building volume density [8], sky view factor [9,10], and building height [11] have been explored in contemporary investigations. Recent studies have focused on how the morphology of urban fabric affects LST [12,13]. Metrics such as the total ISF and the urban or green vegetation index [14] have been utilized in [15,16] and [14], respectively. Rasul et al. [17] and Azmi et al. [18] focus on the relationship between LST and urban morphology derived from LCZs classification, exhibiting overheating in the densest LCZs.

Most of the studies mentioned above used Landsat 8 (L8) images, focusing on a short time series that only included detections during either daytime or nighttime hours, due to its temporal resolution, which is approximately 16 days. As reported by [19,20], the low temporal resolution of the Landsat is not suitable for studying the dynamics of urban LST during specific meteorological conditions, such as heat waves (HWs). Garcia et al. [21] combines air quality, SUHII, and LST during HWs and compares them with normal climatic conditions. As reported by the authors, this relationship is influenced by a range of factors, including local climate, geographical location, and the specific morphology of each city [21–23]. However, studies exploring SUHII and actual urban geometry considering HW periods are still scarce in the literature, especially using Sentinel-3 data and involving Mediterranean cities.

The main objective of this study is to examine the relationship between SUHII, derived from Sentinel-3 LST data, and detailed urban morphological parameters for two Italian cities: Milan and Lecce. Additionally, the study aims to identify the primary morphological drivers influencing SUHII through multiple linear regression analysis. For this purpose, over 1000 satellite images were collected, focusing on the winter (December, January, and February) and summer (June, July, and August) seasons of 2022–2023. After a quality assessment, 264 images were selected for Lecce's summer season and 163 for its winter season, while for Milan, 212 images were selected for the summer season and 132 for the winter season. Further details on the image quality check process are provided in the following sections. These images were used to analyze how SUHII correlates with the specific urban geometries, including the following: the average impervious surface fraction (ISF), height of buildings (HM), aspect ratio (AR), sky view factor (SVF), and building surface fraction (BSF). According to Joshi et al. [24], a range of factors influences the intricate interaction between urban overheating and heat waves. Key elements include urban

geometry, land use, and built-up area density, which collectively play a significant role in this phenomenon. For instance, the prevalence of large impervious surfaces enhances heat retention due to materials with high thermal capacity, while urban compactness contributes to heat trapping and restricts airflow. In densely urbanized areas, these conditions trigger feedback mechanisms, notably intensified by the extensive use of cooling/heating systems, which increase the sensible heat flux at canyon level, especially during HWs. Further research is necessary to comprehensively understand the contributory aspects of these factors across diverse urban contexts, at both microclimatic and macroclimatic scales, to support effective urban planning and mitigate the adverse impacts of heat waves on urban populations. Moreover, the study focuses on HW periods to assess the impact of extreme weather events on SUHII evaluating intracity thermal differences to identify the most vulnerable areas. This study utilizes sea and land surface temperature radiometer (SLSTR) data from the Copernicus Open Access Hub (https://dataspace.copernicus.eu/, accessed on 6 September 2024) processed with a split-window algorithm on the S8 and S9 bands to deliver LST products.

Using Sentinel-3 for this SUHII analysis offers innovative advantages over traditional satellite sources, such as Landsat and MODIS, which are commonly used in similar studies [25]. Unlike Landsat, Sentinel-3 provides higher temporal resolution with its daily revisit and dual morning-evening imaging, allowing it to capture diurnal temperature variations. This capability is crucial for observing SUHII dynamics across day and night, especially during HWs, enabling a more continuous and robust assessment of urban heat responses to extreme weather.

Compared to MODIS, Sentinel-3 reduces the risk of view-angle-related distortions that can occur with MODIS's 2330 km swath and wide view angle (often exceeding 50° in summertime analyses). This off-nadir angle can lead to underestimations of SUHII, as shown by Du et al. [26]. In contrast, Sentinel-3's narrower 1400 km swath and more stable center-field precision offer enhanced accuracy, making it particularly suited for high-resolution urban climate studies focused on SUHII during critical heat wave periods. Also, the novelty of this work is in the use of data from Sentinel-3 in combination with the use of real data on urban morphology instead of the classic LCZ. This is confirmed by the small number of articles using Sentinel-3 data. This study uniquely employs Sentinel-3 data to quantify SUHII variability in Mediterranean cities under HW conditions, emphasizing differences between urban forms in Milan and Lecce. By comparing cities with distinct morphologies and climates, the study offers insights into how structural and environmental contexts contribute to SUHII, which is critical for region-specific adaptation strategies.

This information can guide local authorities and urban planners in implementing specific adaptation strategies, such as improving green spaces, optimizing building design, and improving urban practices to mitigate heat island effects.

2. Materials and Methods

In this section, the step-by-step approach undertaken to achieve the objectives is detailed. The data sources utilized, the analytical techniques employed, and the specific procedures followed to analyze the correlations between SUHII and urban morphological parameters are outlined.

2.1. Description of the Study Cities and Selected Areas

The Köppen climate classification system, one of the most widely used climate classification methods worldwide, categorizes climate regions based on local vegetation (source: https://koeppen-geiger.vu-wien.ac.at/, accessed on 1 November 2024). In Milan, the climate is classified as "Cfa," indicating a warm, temperate climate with significant rainfall, including precipitation during the driest month. Urbanistically, Milan is a sprawling metropolis characterized by radial city development, with newer settlements expanding outward from the central core. In contrast, the city of Lecce experiences a typical Mediterranean climate, with mild winters and notably warm and dry summers, classified as "Csa"

in the Koppen classification. Urban development in Lecce follows a radial pattern, originating from the central nucleus and extending along three main directions: northwest, with the industrial area; east, leading toward the coastline; and south, primarily comprising residential areas [25]. The study encompasses two distinct regions. The first region (Figure 1, highlighted in red) focuses exclusively on the urban areas of Milan (Figure 1a) and Lecce (Figure 1c), where various morphological parameters were computed using QGIS software (version: 3.22.1, https://qgis.org/it/site/, accessed on 5 November 2024). The second region (Figure 1a,c, highlighted in blue) extends beyond the urban areas to include the surrounding rural regions. This larger area was selected to enable a robust statistical analysis that includes various land uses. Urban and rural areas were defined by classification at a spatial resolution of 1 km. Urban areas were identified by an ISF exceeding 95%, while rural areas were characterized by a fraction of ISF below 5%. This criterion is essential to accurately estimate the median LST of rural areas (LSTrur). A closer view of the image, on the right panels, reveals zones with a PSF exceeding 95% (Figure 1b, highlighted by green squares).

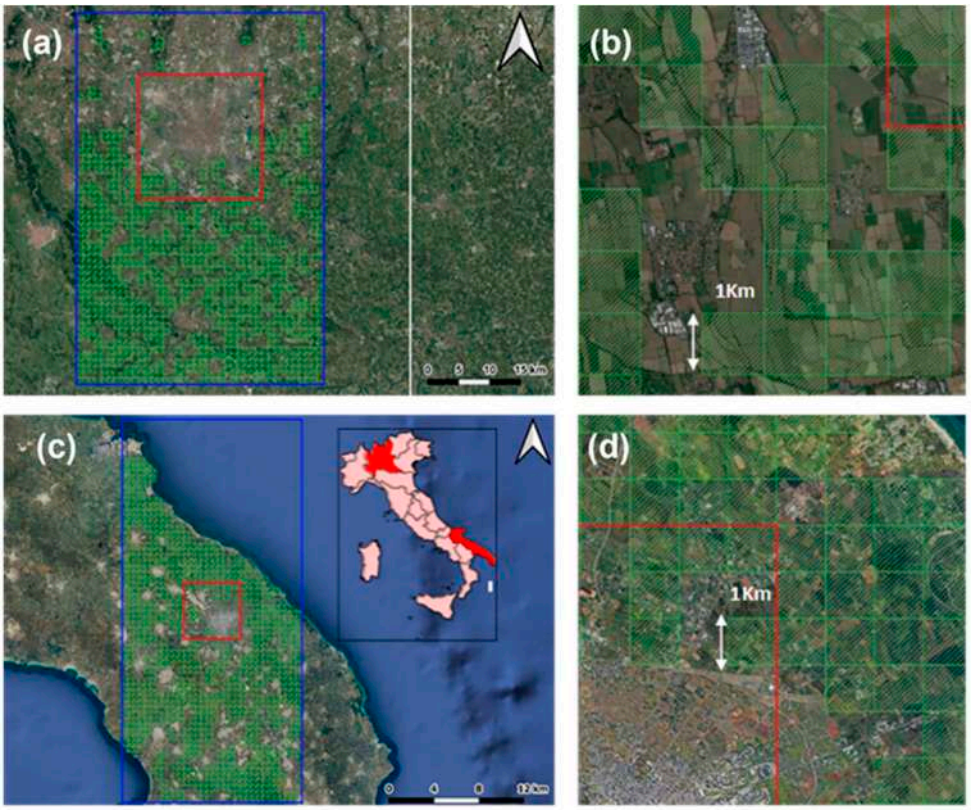

Figure 1. Study areas, with Milan above (**a**) and Lecce below (**c**). Urban areas are highlighted in red, while the blue area delineates regions designated for identifying rural areas. An adjacent zoom-in image (**b**,**d**) displays rural areas identified by a pervious surface fraction (PSF) greater than 95%.

2.2. Morphological Parameters and Land Surface Temperature (LST)

2.2.1. Morphological Analysis

To describe accurately the morphology of the two cities, different morphological parameters have been calculated following the methodology presented in Esposito et al. [27], including HM (the geometric average over a specific area of building heights), AR (the mean height-to-width ratio of street canyons, building spacing), SVF (the ratio of the amount of sky hemisphere visible from ground level to that of an unobstructed hemisphere), BSF (ratio of building plan area to total plan area), ISF (ratio of impervious plan area to total plan area), and PSF (ratio of pervious plan area to total plan area):

- HM has been calculated using the following formula:

$$HM = \frac{\Sigma_{i=1}^{N} H_i}{N} \quad (1)$$

where H_i is the height of building i and N is the total number of buildings in the cell of the grid.

- SVF has been calculated using the Urban Multi-scale Environmental Predictor (UMEP) (https://umep-docs.readthedocs.io/en/latest/index.html, accessed on 14 June 2024), a climate service tool tailored for researchers and professionals in fields such as architecture, climatology, energy, health, and urban planning. UMEP is implemented as a plugin for QGIS and facilitates the pixel-wise generation of SVF through ground and building models. The methodology employed for calculating SVF in this study is detailed in the work of Lindberg and Grimmond [28].
- The formula for AR was derived from the SVF formula that can be also expressed as "$\cos(\arctan(2 \times AR))$" [29], and, consequently, AR was calculates as follows:

$$AR = 0.5 \times \sqrt{\left(\frac{1}{SVF}\right)^2 - 1} \quad (2)$$

- BSF, ISF and PSF were calculated with the following formula:

$$\frac{\Sigma_{1=1}^{N} A_i}{A_T} \quad (3)$$

where A_i refers to the building plan area (in the case of BSF), impervious plan area (in the case of ISF) or permeable plan area (in the case of PSF), while A_T is the total area of the cell.

To enable comparison with Sentinel-3 LST data, a spatial resolution of 1 km was used to calculate the morphological parameters, which have been derived from two distinct datasets: HM, AR, SVF, and BSF from vector datasets (SIT Puglia—http://www.sit.puglia.it, accessed on 14 September 2024 and Milano Geoportale—https://geoportale.comune.milano.it, accessed on 17 September 2024), while ISF and PSF from the CLC + Backbone 2021 (https://land.copernicus.eu/en/products/clc-backbone/clc-backbone-2021, accessed on 1 November 2024). An overview of the morphological parameters, specific to the urban areas for both cities is provided in Table 1. In the urban area of Milan, buildings have a mean (spatially averaged) height HM of 10.20 m, which is taller than in Lecce (6.50 m), suggesting denser urban development with a higher BSF (0.14 on average) compared to Lecce (0.05). Conversely, Milan exhibits a lower SVF (0.89 on average), indicating fewer open spaces throughout the urban area, while Lecce has a higher SVF (0.96 on average). Consequently, the AR pattern (mean value 0.23) is inverted, indicating narrower street canyons than in Lecce, which has a lower mean value (0.08). Milan also has a higher mean ISF (0.49), indicating more impervious surfaces, while Lecce has a higher permeable surface fraction (PSF) (0.74), indicating more green spaces. These differences reflect variations in urban morphology between the two cities.

2.2.2. Satellite Images and Land Surface Temperature

Surface temperatures have been acquired by the Level-2 LST product of the Sentinel-3 satellite (S3A and S3B). These data consist of daily daytime and nighttime thermal images at a spatial resolution of 1 km. In addition to LST values, cloud cover information has also been included. The Sentinel Application Platform (SNAP) software provided by ESA Earth Online (version 9.0.0, https://earth.esa.int/eogateway/tools/snap, accessed on 15 September 2024) has been utilized to process the acquired data. A quality check has been performed on the processed images to avoid the effect of cloud cover on LST. Specifically, all images with a cloud cover greater than 10% have not been considered, while, for images

with any cloud presence, a 3 km buffer was created around the cloudy areas to exclude LSTs affected by cloud shading. Furthermore, SUHII outliers above the 10th and 90th percentile have not been selected in the following analyses. This approach provides an ideal framework for the analysis in this work, which relies on mean values and could be significantly affected by outliers.

Table 1. Mean values(spatially averaged), minimum values, maximum values, and standard deviations of morphological parameters over the urban areas of Milan and Lecce.

Milan Urban Area						
	HM (m)	SVF	AR	BSF	PSF	ISF
Mean	10.20	0.89	0.23	0.14	0.51	0.49
Max	23.60	1.00	1.11	0.51	1.00	0.96
Min	3.00	0.48	0.00	0.00	0.04	0.00
dv.std	4.10	0.11	0.22	0.11	0.28	0.28
Lecce Urban Area						
	HM (m)	SVF	AR	BSF	PSF	ISF
Mean	6.50	0.96	0.08	0.05	0.74	0.26
Max	15.5	1.00	0.73	0.45	1.00	0.92
Min	1.50	0.63	0.00	0.00	0.09	0.00
dv.std	2.80	0.06	0.12	0.09	0.24	0.24

The dataset consists of 264 images for Lecce (70 during HWs) and 212 images for Milan (73 during HWs), collected over the above-mentioned period. This includes multiple daytime and nighttime LST images obtained for almost every day. It is worth emphasizing that the number of HWs in the subsequent analysis is lower than indicated above due to the quality control.

The HW phenomena have been identified using the warm spell duration index (WSDI), which represent the annual count of days when the daily maximum temperature remains above the 90th percentile (at least for 3 consecutive days), based on the period of 1991–2020 (5-day window) [30–33]. These extreme events have been identified for the summer (June, July, and August—JJA) of 2022 and 2023. Specifically, SUHII is defined as the difference between urban (LSTurb) and median rural temperatures (LSTrur):

$$\mathrm{SUHII} = \mathrm{LSTurb} - \mathrm{LSTrur} \tag{4}$$

To improve the readability of the results and to allow inter-comparison between the two cities, the different morphological parameters have been normalized (HM* and AR*) according to Equation (5), while a reverse SVF has been implemented to ensure consistency with other parameters, without affecting the magnitude of SVF parameter. The normalized factor x* was obtained according to:

$$x^{*} = (x - \min(x))/(\max(x) - \min(x)) \tag{5}$$

where x is the original value, min(x) is the minimum value in the dataset, and max(x) is the maximum value in the dataset. In addition, to better describe and detail SUHII phenomena, a micrometeorological station at a suburban area of Lecce was considered, where soil moisture was measured throughout the analyzed period [34].

2.3. Multicollinearity Analysis and Multiple Linear Regression

To better understand the relationships between urban morphology and SUHII, a multicollinearity analysis and multiple linear regression was applied to understand the main drivers influencing SUHII [35].

2.3.1. Variance Inflation Factor (VIF) Calculation

VIF analysis is used to identify and quantify multicollinearity among the independent variables of a multiple linear regression model. Multicollinearity occurs when an independent variable is highly correlated with one or more of the other independent variables, which can adversely affect the accuracy and interpretation of the regression model. For each variable, the VIF is calculated as follows:

$$\mathrm{VIF}(x_i) = \frac{1}{1 - R_i^2} \tag{6}$$

where R_i^2 is the coefficient of determination of the regression of x_i on the other independent variables. R_i^2 is calculated using the following equation:

$$R_i^2 = 1 - \frac{\mathrm{SSR}}{\mathrm{SST}} \tag{7}$$

where SSR is the sum of residual squares (the part of x_i not explained by the other variables) and SST is the total sum of squares.

If R_i^2 is close to 1 (high correlation with the other variables), then VIF(x_i) will be very large. A high VIF indicates that the variable is strongly collinear with the others. Thus:

- VIF(x_i) = 1 indicates that there is no correlation between xi and the other independent variables.
- VIF(x_i) > 1 indicates that there is some collinearity.
- Values of VIF(x_i) greater than 10 are often considered problematic because they indicate too high a level of collinearity.

2.3.2. Multiple Linear Regression

Multiple linear regression is a statistical technique utilized to model the relationship between one dependent variable and multiple independent variables. This method enables the analysis of more complex relationships among variables. The mathematical representation of multiple linear regression is expressed as follows:

$$Y = \beta_0 + \beta_1 X_1 + ...\beta_n X_n + \epsilon \tag{8}$$

where Y denotes the dependent variable (SUHII), X_1, X_2,. . ., X_n represent the independent variables (morphological parameters), β_0 is the intercept, β_1, β_2,. . ., β_n are the coefficients associated with the independent variables, and ϵ signifies the error term that accounts for the variability in Y not explained by the independent variables.

Multiple linear regression is advantageous for understanding the relationships among variables, as it facilitates the exploration of how various independent variables impact the dependent variable, allowing for the identification of key factors influencing outcomes. Additionally, the model serves as a predictive tool, enabling the estimation of the dependent variable based on known values of the independent variables.

Results are presented and discussed in the following sections.

3. Results

3.1. SUHII Seasonal Characterization

The SUHI values have been classified into two subsets to represent the winter (December, January, and February—DJF) and JJA seasons (as defined previously). Furthermore, each dataset has been further divided into two subsets to evaluate the average SUHII

during the day (based on satellite passages between 8:00 and 10:00 local time) and the night (between 20:00 and 22:00 local time). The results indicate that during the JJA season, Milan experiences mean daytime SUHII values of 4.25 °C and nighttime values of 1.92 °C. The highest SUHI peaks were recorded in July and August of 2022 and August 2023, with peak values of 6.52 °C, 6.24 °C, and 5.77 °C, respectively. In contrast, Lecce has an average daytime SUHII of −1.08 °C and nighttime SUHII of 0.72 °C. Lecce's highest SUHII peaks occurred in June and August of 2023, with values of 1.65 °C and 1.02 °C, respectively, while August 2022 also showed significant peaks around 1.20 °C. During the DJF season, Milan's average SUHII values are 2.13 °C during the day and 0.95 °C at night. The highest SUHII values were observed in February of both 2022 and 2023. Conversely, Lecce records average daytime and nighttime SUHII values of −0.28 °C and 0.32 °C, respectively.

Seasonal analyses show that SUHII tends to be higher during JJA in both cities, except for the negative values that occur for Lecce, with the latter more pronounced during this period. This type of phenomenon is known as surface urban cool island (SUCI) [17], will hereafter be referred to as "negative SUHII" for the purposes of this paper. This aspect will be analyzed in detail in the next sections.

3.2. Relationships Between Urban Morphology and SUHII in Summertime

Figure 2 illustrates the SUHII values as a function of specific morphological parameters, separated into daytime (top) and nighttime (bottom) for both Milan and Lecce. In the graphs, the morphological parameters are grouped into 0.10 large bins, although a few cases involved bins larger than 0.10 to include more values. The bin size width was estimated to obtain the average values based on robust statistics but without losing detail on the trend of the parameter considered.

In Milan, quadratic relationships (Table 2) are observed during the day (Figure 2a), where parameters such as SVF, BSF, and AR* exhibit large SUHII (above 5.00 °C) for values ranging between 0.20 and 0.25. Beyond this threshold, SUHII reaches a plateau at about 6.00 °C. Conversely, ISF and HM* exhibit an initial temperature increase (about 3.00 °C) in the first phase (up to 0.4), then stabilizes to an average increase of about 1.00 °C. Analysis of the individual parameters reveals that high values of BSF, AR* (narrower road canyons), ISF, and SVF correspond to higher temperature anomalies, with peaks between 6.00 and 7.00 °C. The nighttime data for Milan (Figure 2c) show a similar trend, with maximum SUHII values reaching 4.50 °C. Linear relationships for parameters like ISF and HM* suggest that SUHII values increase by approximately 0.80 °C for every 0.20 increase in these morphological parameters.

Diurnal data from Lecce (Figure 2b) present a different scenario, according to the seasonal analysis. The observed relationships contrast with previous cases, with higher values of morphological parameters corresponding to lower thermal anomalies, and vice versa. Quadratic relationships are observed for SVF and AR while linear relationships were predominant for ISF, BSF, and HM* (Table 2). Specifically, for SVF and AR*, there was an initial decrease of approximately 2.00 °C, followed by a mean decrease of 0.50 °C until reaching a plateau.

Conversely, ISF, BSF, and HM*, characterized by linear relationships, showed a slight increase, with values between 0.30 and 0.70 °C (Table 2). In Lecce, the nighttime data (Figure 2d) follow a trend like Milan, but with weaker thermal anomalies, slightly above 2.00 °C. Quadratic relationships are evident for SVF and AR*, with the latter reaching a plateau at morphological values above 0.40, corresponding to anomalies of 2.00 °C. For these parameters, there is an initial temperature increase of about 1.50 °C, which then stabilizes to an increase of approximately 0.50 °C. In contrast, linear relationships are observed for BSF, ISF, and HM*, showing a consistent rise in SUHII as the parameter value increases by 1.00 °C for BSF and 0.40 °C for ISF and HM*.

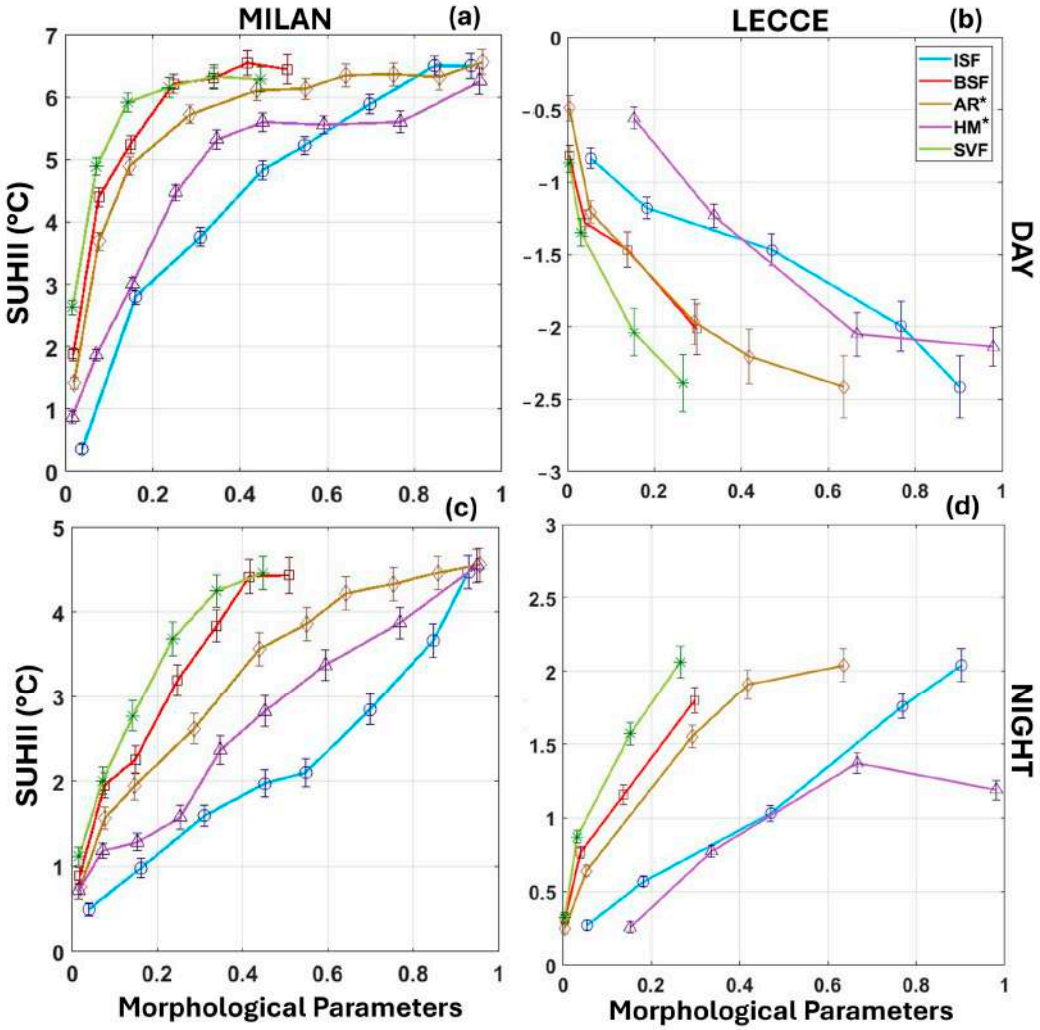

Figure 2. Daytime (**a**,**b**) and nighttime (**c**,**d**) SUHII as a function of different urban morphological parameters for the two cities; values refer to summer period. Error bars represent the standard error, which is between 0.10 °C and 0.20 °C.

Table 2. Polynomial fits (with the respective coefficients and the Pearson coefficient R^2) for the scatter plots between SUHII and morphological parameters for Lecce and Milan; the data analysis refers to JJA period.

	Milan	
	Daytime	Nighttime
ISF	$y = -7.29x^2 + 13.42x + 0.25$ $R^2 = 0.9811$	$y = 4.11x + 0.21$ $R^2 = 0.9656$
BSF	$y = -33.23x^2 + 25.09x + 2.02$ $R^2 = 0.9361$	$y = -10.37x^2 + 12.63x + 0.77$ $R^2 = 0.9852$
AR*	$y = -9.05x^2 + 12.53x + 2.36$ $R^2 = 0.8661$	$y = -4.38x^2 + 8.09x + 0.78$ $R^2 = 0.9939$
HM*	$y = -9.97x^2 + 14.5x + 0.98$ $R^2 = 0.9485$	$y = 4.12x + 0.76$ $R^2 = 0.9851$
SVF	$y = -39.35x^2 + 24.96x + 2.75$ $R^2 = 0.9016$	$y = -18.03x^2 + 16.03x + 0.89$ $R^2 = 0.9991$

Table 2. *Cont.*

	Lecce	
	Daytime	Nighttime
ISF	$y = -1.71x - 0.76$ $R^2 = 0.9752$	$y = 2.06x + 0.14$ $R^2 = 0.9951$
BSF	$y = -3.62x - 0.95$ $R^2 = 0.9234$	$y = 4.69x + 0.44$ $R^2 = 0.9606$
AR*	$y = 5.21x^2 - 6.02x - 0.66$ $R^2 = 0.9601$	$y = -4.97x^2 + 5.94x + 0.27$ $R^2 = 0.9969$
HM*	$y = -2.47x - 0.31$ $R^2 = 0.9611$	$y = 1.87x + 0.03$ $R^2 = 0.9672$
SVF	$y = 19.34x^2 - 10.64x - 0.91$ $R^2 = 0.9821$	$y = -16.69x^2 + 10.64x + 0.39$ $R^2 = 0.9768$

3.3. Relationships Between Urban Morphology and SUHII in Wintertime

During the DJF season, the intensity of the Lecce SUHII showed values above −1.00 °C even in the most densely urbanized areas. The relationships indicated that a greater morphological parameter corresponds to stronger negative thermal anomalies, showing linear associations (Table 3), even if the SUCI intensity is weaker than in summer. All parameters, except for ISF, show a decrease rate of 0.5 °C, while ISF has a decrease rate of 0.20 °C. In the case of Milan, insufficient daytime data were available due to extensive cloud cover, which made satellite images unusable for analysis.

Table 3. Polynomial fits (with the respective coefficients and the Pearson coefficient R^2) for the scatter plots between SUHII and morphological parameters for Lecce and Milan; the data analysis refers to DJF period.

	Milan	
	Daytime	Nighttime
ISF	---	$y = 4.14x^2 - 1.57x + 0.35$ $R^2 = 0.9251$
BSF	---	$y = 4.15x^2 + 4.29x + 0.16$ $R^2 = 0.9544$
AR*	---	$y = 3.17x + 0.18$ $R^2 = 0.9895$
HM*	---	$y = 2.76x^2 + 0.53x + 0.24$ $R^2 = 0.9897$
SVF	---	$y = 6.30x + 0.19$ $R^2 = 0.9946$
	Lecce	
	Daytime	Nighttime
ISF	$y = -0.88x + 0.07$ $R^2 = 0.9822$	$y = 0.95x^2 + 0.54x - 0.02$ $R^2 = 0.9903$
BSF	$y = 6.74x^2 - 4.01x + 0.01$ $R^2 = 0.9902$	$y = 3.16x + 0.06$ $R^2 = 0.9705$
AR*	$y = 1.02x^2 - 1.79x - 0.01$ $R^2 = 0.9787$	$y = -2.83x^2 + 3.80x - 0.03$ $R^2 = 0.9994$
HM*	$y = 1.36x^2 - 2.15x + 0.38$ $R^2 = 0.9896$	$y = -2.11x^2 + 3.17x - 0.45$ $R^2 = 0.8832$
SVF	$y = 5.62x^2 - 4.06x + 0.003$ $R^2 = 0.9979$	$y = -11.31x^2 + 7.10x + 0.01$ $R^2 = 0.9904$

Figure 3b displays the nighttime DJF data in Milan, where linear relationships between SUHII and AR* and SVF are observed. SUHII reaches just above 3.00 °C at higher parameter values, with AR* and SVF showing consistent increases of 0.60 °C and 1.00 °C, respectively. The remaining parameters show a quadratic relationship, where, except for BSF, increasing rates are observed for high values of morphological parameters, also more than 1 °C. Nighttime data for Lecce (Figure 3c) show similar but less pronounced patterns, with maximum SUHII values just over 1.00 °C. Predominantly quadratic relationships indicate a strong initial temperature increase of around 0.70 °C in the early steps, followed by more gradual changes of just over 0.30 °C. In contrast, for BSF, which exhibits a linear relationship, there is a steady increase of 0.60 °C.

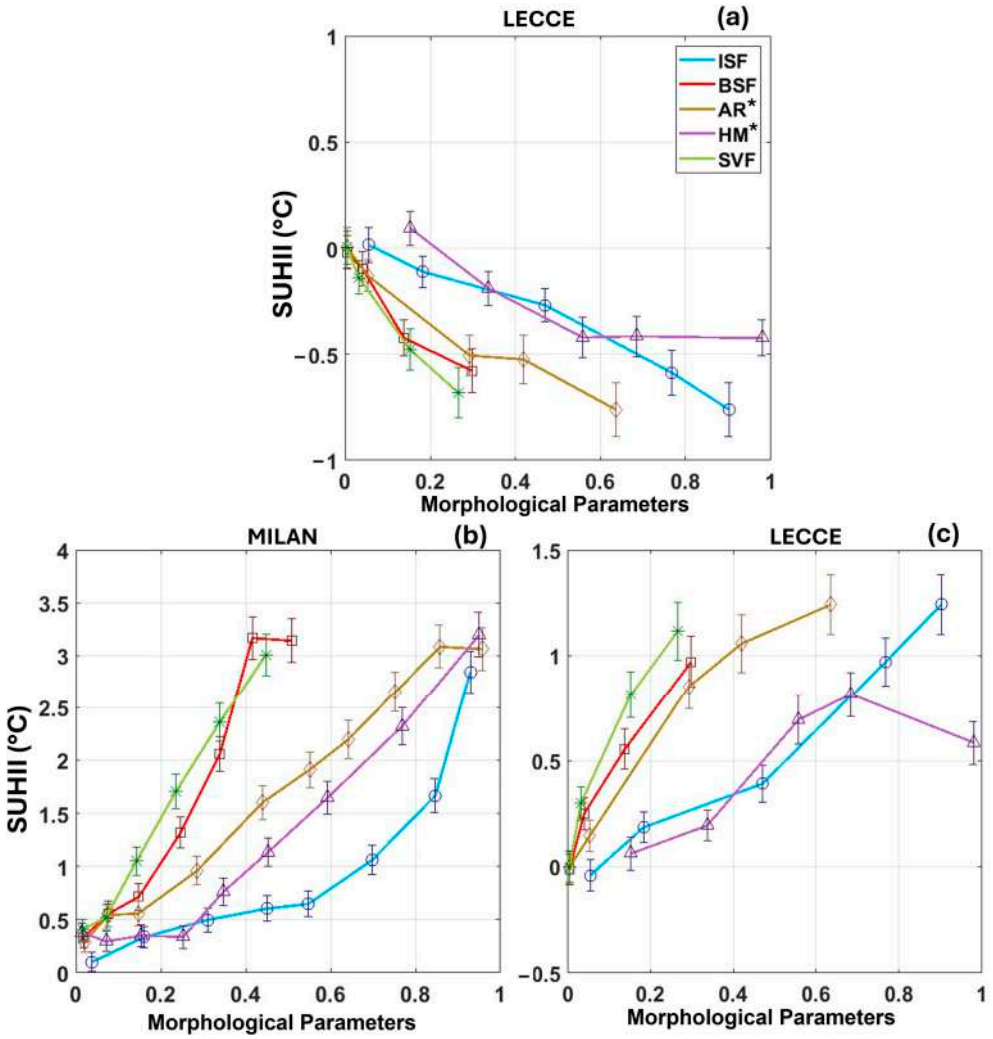

Figure 3. Daytime (**a**) and nighttime (**b**,**c**) SUHII as a function of different urban morphological parameters for the two cities; values refer to winter period. Error bars represent the standard error, which is between 0.10 °C and 0.20 °C.

3.4. Results of Multicollinearity and Multiple Linear Regression

To clarify the influence of morphological parameters on SUHII, a comprehensive analysis was performed to assess the relationship between independent variables (morphological parameters) and the dependent variable (SUHII) through VIF assessment and multiple linear regression analysis.

The VIF calculation showed the following values for Lecce: BSF (15.30), AR (397.48), SVF (345.74), ISF (9.92), and HM (2.72). Similarly, in Milan: BSF (15.28), AR (329.57), SVF (325.33), ISF (10.53), and HM (3.35). After the calculation of VIF for the system of

variables, only the highly correlated components, represented by SVF (Lecce: 345.74; Milan: 325.33) and AR (Lecce: 397.48; Milan: 329.57), were excluded based on their high levels of correlation. In the remaining set of variables (BSF, HM, and ISF), a VIF threshold of 12 was applied to manage and reduce correlation, leading to the exclusion of BSF (Lecce: 15.30; Milan: 15.28), which is highly correlated with ISF (Lecce: 9.92; Milan: 10.53).

After excluding variables with VIF values over 12, multiple linear regression analyses were conducted separately for both daytime and nighttime scenarios in each city. In the daytime analysis for Lecce, the estimated coefficients for ISF and HM were −2.5 and −0.09, respectively, with corresponding p-values of 3.57×10^{-9} and 6.4×10^{-4}, indicating strong statistical significance. In contrast, the daytime analysis for Milan yielded estimated coefficients of −0.26 for ISF and −0.003 for HM, with p-values of 0.18 and 0.72, respectively, suggesting a lack of statistical significance for these variables.

For the nighttime analysis in Lecce, the estimated coefficients were 2.1 for ISF and −0.002 for HM, with p-values of 3.3×10^{-14} and 0.89, respectively, indicating substantial statistical significance for ISF. In Milan's nighttime case, the coefficients were 1.3 for ISF and 0.05 for HM, with p-values of 1.7×10^{-12} and 3.1×10^{-13}, respectively, further demonstrating strong significance for the ISF variable in this context.

3.5. Day-Night SUHII Variations in Heatwave and Non-Heatwave Conditions

The HWs occurring during the JJA of 2022 and 2023 were identified utilizing percentile climatology, as outlined in Section 2.2.2. Specifically, for the city of Lecce, a total of five HWs were identified, with the longest lasting 13 days:

- Three HWs occurred during the summer of 2022 (1st to 6th June, 28th June to 5th July, and 23rd to 26th July).
- Two HWs were recorded in the summer of 2023 (12th to 25th July and 26th to 28th August).

In the case of Milan, nine HWs were identified, with the maximum duration being 11 days:

- Six HWs were observed during the summer of 2022 (2nd to 6th June, 12th to 20th June, 2nd to 7th July, 14th to 16th July, 20th to 26th July, and 1st to 6th August).
- Three HWs were identified in the summer of 2023 (9th to 11th July, 16th to 19th July, and 14th to 25th August).

In Figure 4, the "HW" box represents a series of days during the heatwave (HW) period. The non-heatwave (NHW) period is defined by selecting a set of days with normal climatic conditions, matching the length of the HW period, both before and after the heatwave. "HW_22" and "NHW_22" refer to the heatwave and non-heatwave periods in 2022, while "HW_23" and "NHW_23" refer to those in 2023. In both years, the suffixes "a" and "b" indicate the first and second HW or NHW periods, where applicable.

In Milan, during the HW_22 period, the range of diurnal SUHII values (Figure 4a) is lower than in the corresponding NHW_22 period, although their mean values are quite similar: 3.94 °C during HW and 4.11 °C during NHW. On the contrary, in HW_23, the mean SUHII value is higher than during NHW_23, at 4.25 °C and 3.99 °C, respectively. The situation is markedly different at night (Figure 4c), where the SUHII effect is more pronounced during HW periods, when the range of nighttime SUHII values consistently exceeds that of the NHW periods. During these HW periods, SUHII averages above the NHW periods in a range between 0.10 and 0.79 °C. For Lecce, the diurnal SUHII values (Figure 4b) exhibit lower mean negative values during all the three HW periods, ranging from −1.74 °C to −1.36 °C. On the contrary, during the night, the average SUHII is higher during all HW periods, in the range of 0.08 to 0.15 °C. Figure 5 illustrates the relationships between SUHII and morphological parameters during all HW and NHW periods, for nighttime data in both cities. All parameter values were normalized for a better comparison between parameters and between the two cities according to Equation (2) in Section 2.2.2.

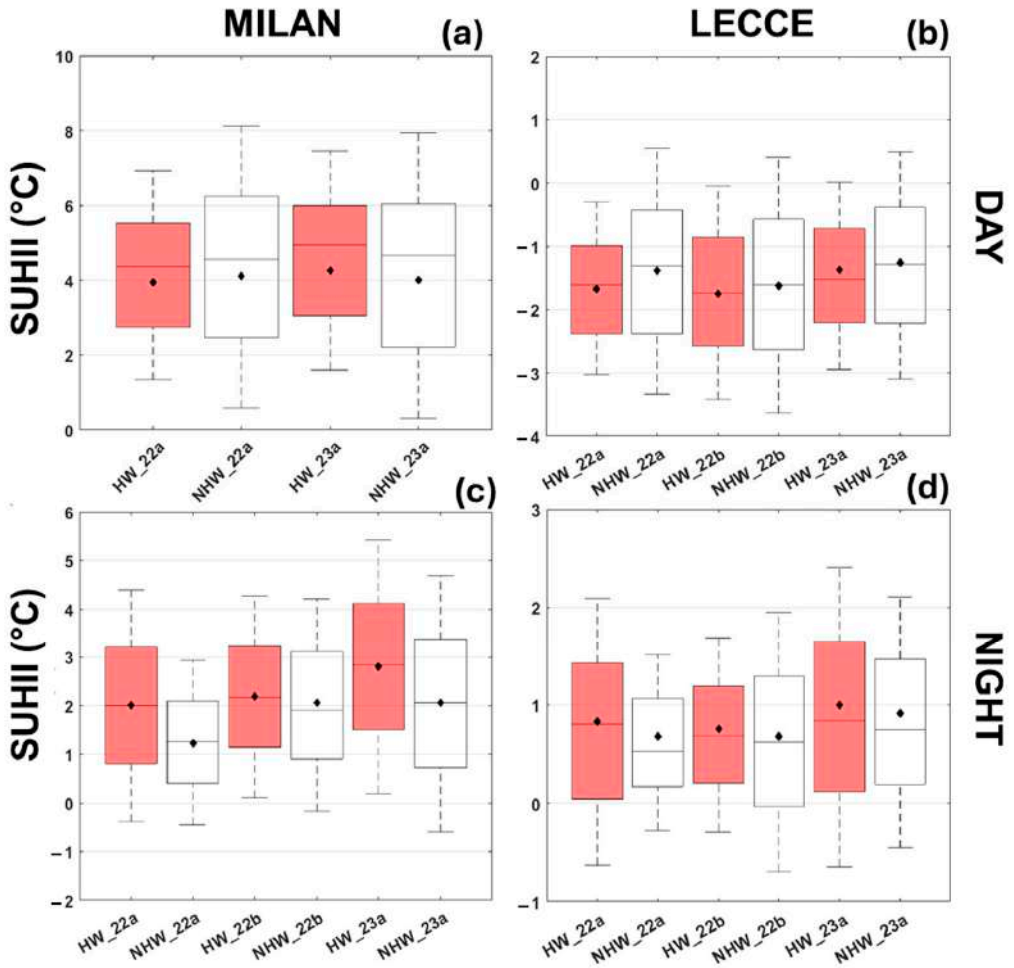

Figure 4. Boxplot of SUHII during HW (in red) and NHW (in white) in Milan (**a**,**c**) and Lecce (**b**,**d**). The black dots indicate the mean values, and the lines are the median values. The boxes represent the 25th and 75th percentiles, while the whiskers correspond to $\pm 2.7\sigma$ and 99.3% data coverage.

Figure 5 shows that SUHII is slightly higher during HW periods in both cities. In Milan, the average difference is 0.35 °C, with a maximum range of 0.52–0.55 °C, corresponding to the highest values of urban parameters such as BSF and AR. In Lecce, the average difference is 0.20 °C, with a maximum range of 0.25–0.27 °C, also associated with BSF and AR. SUHII tends to increase, especially in densely urbanized areas, with this effect being most pronounced in Milan. A consistent pattern emerges in both cities: in less urbanized areas with low morphological parameter values, the differences between HW and NHW conditions are minimal. However, as morphological parameter values reach about 0.20, the HW and NHW data begin to diverge, with the largest disparities occurring at higher parameter values. T-student was applied to these samples for both cities, with results showing that there is no significant difference between SUHII during and in the absence of the HWs. The mean *p*-value for Lecce is 0.75 during the night, while for Milan, it is 0.67.

Similarly to the previous analysis, Figure 6 illustrates the SUHII data for the city of Lecce during daytime. During HW periods, negative SUHII effect appears to intensify, with an average temperature difference of −0.30 °C and a maximum difference of −0.70 °C, which corresponds to the highest values of parameters such as SVF and AR. All parameters exhibit a consistent trend, showing larger differences only at higher values of urban morphological parameters. Indeed, as parameter values increase to around 0.20, a divergence between the HW and NHW data becomes important, reaching maximum disparities at higher parameter values (approximately 0.40 °C). T-student was also applied in this case,

resulting in the finding that there is no significant difference between the two groups, with *p*-values ranging from 0.45 to 0.62.

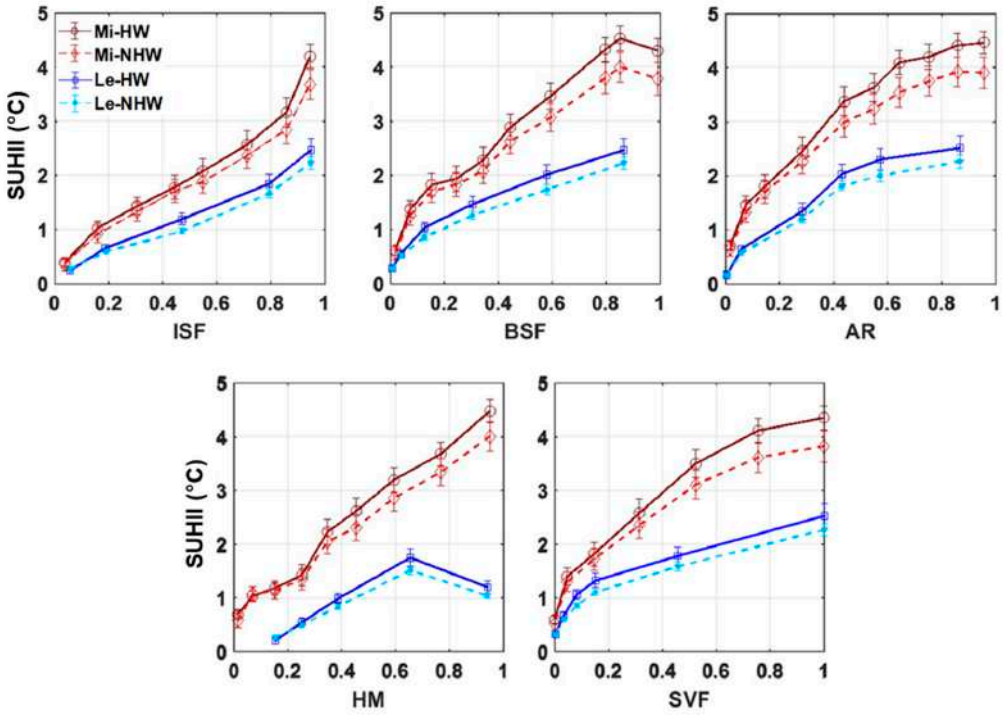

Figure 5. SUHII as a function of urban morphological parameters in Lecce and Milano during HW (continuous line) and NHW (dashed line) periods for ISF, BSF, AR, HM, and SVF (all parameter values were normalized); values refer to nighttime. Error bars represent the standard error, which is below 0.20 °C.

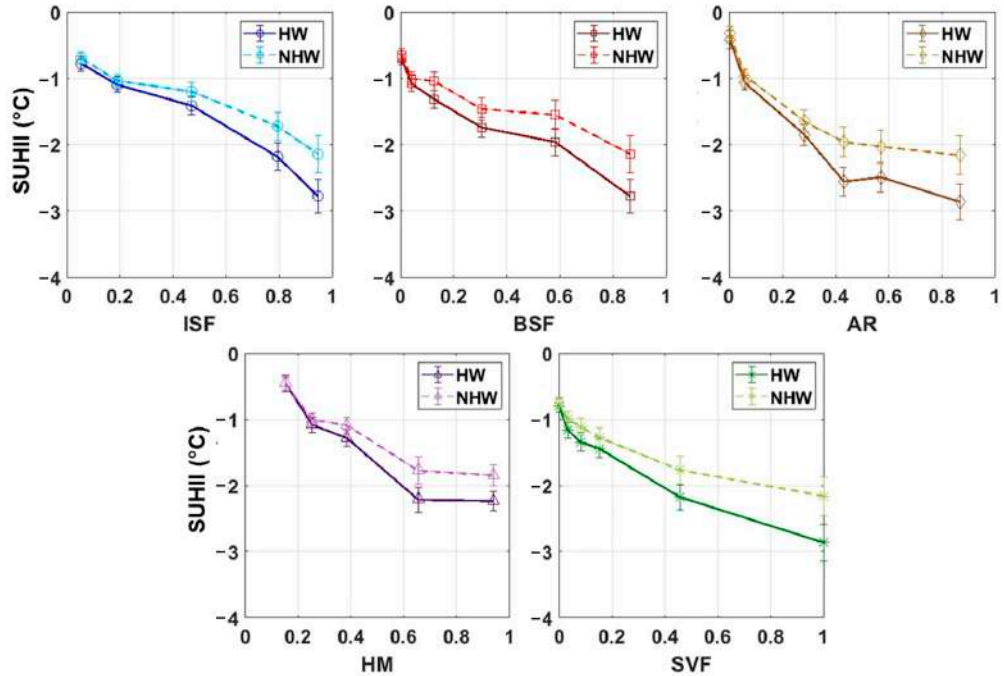

Figure 6. As in the Figure 6, but during daytime in the city of Lecce. Error bars represent the standard error, which is below 0.20 °C.

To assess the impact of the HW on the distribution of SUHII, Figure 7 shows the difference between the average SUHII during HW and NHW for the city of Milan during night (Figure 7a) and Lecce (Figure 7b) during daytime. This analysis enables the identification of areas most vulnerable to the SUHII enhancement during HWs. Daytime data from Milan and nighttime data from Lecce are not shown because no significant differences were observed. This is supported by the *t*-test results, with *p*-values of 0.26 for Milan and 0.75 for Lecce, indicating a lack of statistical significance.

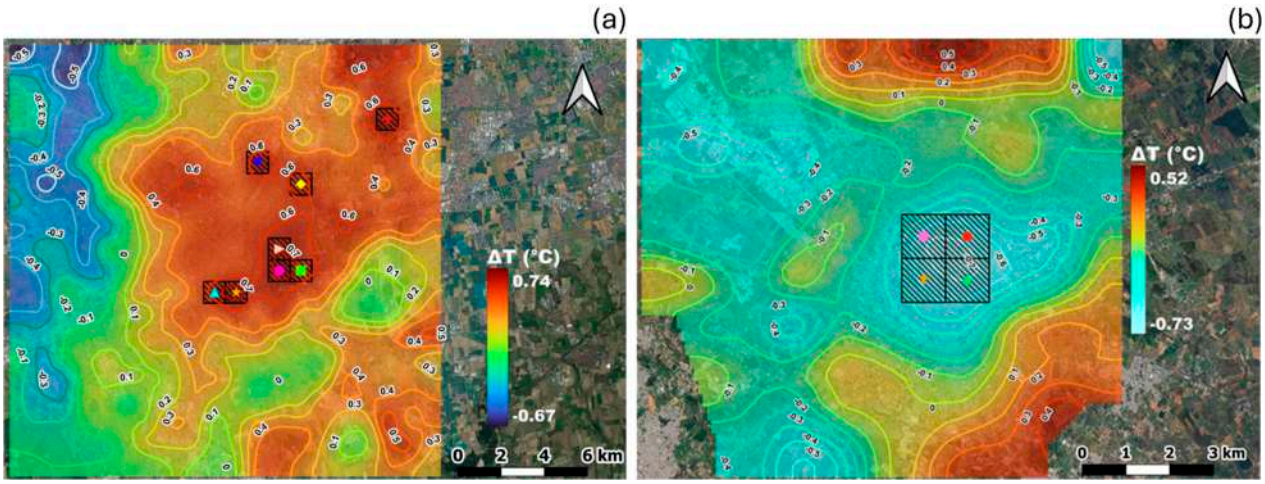

Figure 7. Differences in mean SUHII during HWs and NHWs for the city of Milan during nighttime (**a**) and the city of Lecce during daytime (**b**). Black squares indicate areas with differences above/below than 0.70 °C, respectively.

Figure 7a displays that the city center consistently experiences average temperature anomalies of more than 0.40–0.50 °C, with peaks around 0.80 °C. The areas that seem to be most affected by extreme phenomena are the most densely urbanized areas, as they show AR, BSF, HM, and ISF values above the 75th percentile and SVF and PSF values below the 25th percentile respect to the whole city (Table 4). It should be noted that in some cases, these values are above/below the 90th/10th percentile, referring to areas of the city with peculiar geometric characteristics. Conversely, suburban areas appear less impacted by HWs, showing almost zero values, being characterized by higher percentages of pervious surfaces and overall urban greening. Also in this case, T-student was applied to the entire area, resulting in the finding that there is significant difference with a *p*-value of 0.027.

Table 4. Morphological parameters of areas most susceptible to SUHII in Milan; resolution: 1 km × 1 km.

ID	AREA	HM (m)	BSF	SVF	AR	ISF	PSF	ΔT (°C)
1	▲	13.75	0.35	0.68	0.63	0.87	0.13	0.74
2	▼	12.63	0.25	0.74	0.51	0.81	0.19	0.80
3	✚	11.86	0.17	0.84	0.34	0.67	0.32	0.76
4	■	10.44	0.21	0.91	0.20	0.81	0.20	0.70
5	●	15.87	0.31	0.66	0.67	0.86	0.14	0.79
6	◆	13.94	0.33	0.69	0.61	0.92	0.09	0.72
7	▶	16.70	0.31	0.68	0.66	0.84	0.15	0.71
8	★	14.77	0.23	0.79	0.44	0.69	0.30	0.80

As in the Milan analysis, in Lecce the differences in the average SUHII during HW and NHW periods during daytime are shown in Figure 7b. The central areas of Lecce, which are the most urbanized, display the highest temperature anomalies, averaging around −0.50 °C and reaching peaks of −0.80 °C. The analysis indicates that areas most affected by the cool island effect are primarily within the core of the city, including Lecce's historic center. These areas show SUHII below −0.65 °C, which are characterized by morphological characteristics greater than the 90th (BSF, AR, HM and ISF) percentile and others less than the 10th percentile (SVF and PSF), typically values of dense urban areas (Table 5). T-student applied for the entire area provides *p*-values of 0.26 that means non-significant difference occurred.

Table 5. Morphological parameters of areas most susceptible to SUHII in Lecce; resolution: 1 km × 1 km.

ID	AREA	HM (m)	SVF	AR	BSF	ISF	PSF	ΔT (°C)
1		10.81	0.82	0.35	0.23	0.78	0.23	−0.70
2		15.07	0.63	0.73	0.38	0.92	0.09	−0.75
3		10.42	0.84	0.31	0.20	0.72	0.27	−0.78
4		11.28	0.74	0.54	0.45	0.88	0.12	−0.66

4. Discussion

The findings of this study reveal a pronounced influence of urban morphology on SUHII in Milan and Lecce, as analyzed using Sentinel-3 satellite data from 2022 to 2023. Milan exhibits significantly higher SUHII values during summer, with an average daytime SUHII of 4.25 °C and nighttime SUHII of 1.92 °C, compared to Lecce's respective averages of −1.08 °C during daytime and 0.72 °C during nighttime. Even in winter, Milan's SUHII remains slightly elevated at night (0.95 °C) compared to Lecce (0.32 °C). During the DJF period for nighttime, Milan exhibited a slight SUHII with maximum values just above 3.00 °C, showing both linear and quadratic relationships. In contrast, Lecce's SUHII was even weaker, just above 1.00 °C. These results are in good agreement with those found in previous studies, such as [36], who reported lower SUHII values in the Guangdong–Hong Kong–Macao Greater Bay Area, with daytime and nighttime SUHII averaging 1.74 °C and 0.54 °C during JJA, respectively, and even lower intensities in winter. Similarly, [37] found regional differences in China, with higher median SUHII values during summer days in the northeastern and southwestern regions, ranging from 2.14 °C to 2.64 °C, and lower nighttime values between 0.56 °C and 1.11 °C.

The relationship between SUHII and urban morphological parameters shows distinct patterns for Milan and Lecce. Higher parameter values are associated with more significant temperature anomalies, indicating denser urban areas, while lower values suggest less urbanized regions with smaller SUHII. When comparing SUHII intensity for the same parameter values, Milan consistently shows higher SUHII levels than Lecce.

Multicollinearity and multiple linear regression analyses enabled a comparison of day and night cases for Lecce and Milan, revealing contrasting results. During the daytime, ISF showed a significant negative effect on SUHII in Lecce, indicating that an increase in ISF is associated with a decrease in SUHII. In contrast, ISF did not have a significant effect in Milan, suggesting variability in its influence based on city context. Similarly, HM exhibited a negative effect on SUHII during the day in Lecce, although the associated *p*-value indicated only marginal significance. In Milan, however, HM showed no significant effect on the dependent variable. At night, ISF demonstrated a significant positive effect in both cities, suggesting that increases in ISF are linked to increases in SUHII during nighttime hours. Conversely, HM in Lecce's nighttime case was associated with a negative but non-significant effect. In Milan, however, HM displayed a significant positive effect on SUHII, highlighting substantial variation in the influence of this variable between locations.

These differences emphasize that urban morphology parameters can exert varying effects on heat island intensity depending on the time of day and city-specific characteristics. The finding that ISF and HM are among the main drivers, compared to other parameters, can be explained by the type of relationship observed (Figures 2 and 3). Both parameters generally exhibit a linear relationship, where SUHII increases consistently as the parameter value rises. In contrast, the other parameters exhibit quadratic relationships, with low but frequent values in peri-urban and suburban areas, while higher values are concentrated in the city center, leading to a plateau. However, Lecce presents a negative SUHII during daytime in both summer and winter, suggesting rural areas are warmer than urban ones, showing a straightforward increase in SUHII with rising parameter values. Particularly during the daytime in both summer and winter, with a more pronounced effect in the summer season, where temperatures are approximately 1.00 °C cooler than in winter. This phenomenon was observed through different cities such as Athens, Greece [38] in October (daytime −2.0 °C, nighttime +3.1 °C) and Phoenix, Arizona, USA [39] in July (daytime −3.8 °C and +1.2 °C nighttime). Recent studies in Doha (Qatar) [40] and Erbil (Iraq) [17] also report consistent negative SUHII values. The study in Doha found SUHII values of −5.8 °C during DJF and −4.8 °C during JJA. The study in Erbil, covering July to September, observed SUHII values ranging from −3.5 °C to −4.6 °C. The authors of the latest study attribute the negative SUHII phenomenon primarily to variations in soil moisture, rather than vegetation cover.

In Lecce, soil moisture data from a micrometeorological station for the 2022–2023 period were analyzed. Previous studies [34] identified soil moisture levels below 0.10 m^3/m^3 during summer from 2017 to 2022, significantly lower than the average of 0.30–0.35 m^3/m^3 seen in Italy and most of Europe [41]. This suggests conditions like desert regions. During heatwaves, low soil moisture levels (below 0.10 m^3/m^3) were associated with the most negative SUHII values, indicating that low soil moisture enhances this phenomenon. In the winter, higher soil moisture levels led to lower negative SUHII values effect (Figure 8b). This pattern is consistent with findings by [17], which noted a strong inverse relationship between surface temperature and wetness index.

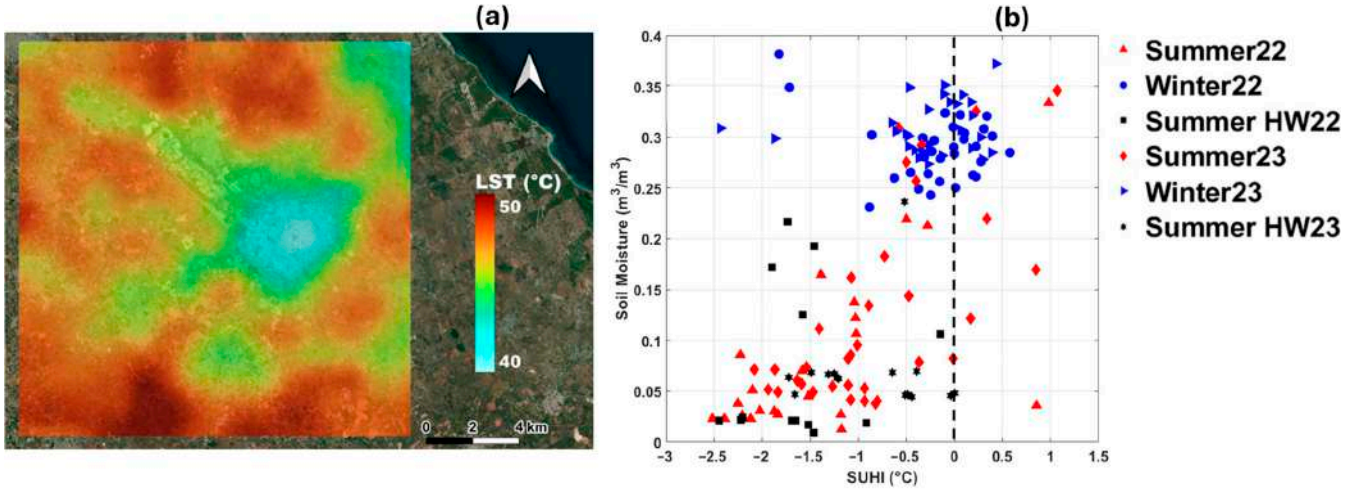

Figure 8. (**a**) Values refer to LST data for 16 July 2023, at 9:34 a.m. showing the SUHII effect on the urban area of Lecce. (**b**) Correlation between soil moisture and daytime SUHII in Lecce, throughout the analyzed period during HW (black symbols) and NHW (red symbols) and for the winter period of 2022 and 2023 (blue symbols).

It is important to note that the historic center of Lecce features light-colored buildings, low-permeability surfaces, and narrow street canyons. Additionally, urban surfaces, including streets and the façades of historic buildings, are made of local white (or at least clear) limestone ("pietra leccese"), which has higher thermal properties [31,42]. The combi-

nation of high albedo and narrow streets, as reported by [43–46], likely contributes to this phenomenon, alongside the effects of the surrounding soil moisture. The negative SUHII observed is consistent with findings of a local air heat island in the city center, which shows negative values during the early summer hours [31].

The analysis of SUHII intensity during HW and NHW periods in Milan and Lecce underscores the impact of extreme weather conditions on urban thermal dynamics, offering crucial insights for urban planning and climate adaptation strategies. A significant difference in SUHII values between daytime and nighttime was observed, particularly during HW periods, with nighttime showing higher SUHII values. This trend highlights the reduced cooling capacity of urban areas during the night, primarily due to heat retention in materials like concrete and asphalt, which release stored heat more slowly. Milan's SUHII values during HW days were higher in 2023 than in 2022, likely influenced by a combination of physical characteristics of the surrounding area and ventilation patterns, emphasizing the dynamic interaction between urban structure and climatic factors.

The pronounced SUHII observed in Milan, especially at night, reflects the role of higher urbanization levels in amplifying thermal stress. In contrast, Lecce, with its lower urban density, exhibits smaller differences between HW and NHW periods, suggesting that urban design and planning, including green infrastructure, can mitigate HW impacts. The relationship between SUHII and BSF (Figure 5) further illustrates these dynamics. In both cities, as BSF exceeds 0.4, the divergence between HW and NHW SUHII becomes more pronounced, with Milan experiencing the largest differences, reaching up to 0.50 °C. This finding aligns partially with [21], which noted SUHII increases of 2.60 °C during daytime and 2.80 °C at night in HW periods.

The distinction between Milan, an inland city, and Lecce, influenced by proximity to the sea (~10 km), underscores regional differences in SUHII responses. Milan's densely urbanized city center showed the highest nighttime SUHII during HWs, with temperature differences exceeding 0.40–0.50 °C and peaking at 0.80 °C, while suburban areas with more greenery saw minimal changes. Conversely, Lecce exhibited negative daytime SUHII during HWs in the urban center, with temperature reductions averaging −0.50 °C, attributed to lower urban density and better cooling effects.

These findings underscore the critical role of urban morphology in modulating SUHII intensity during HW and NHW periods, offering insights for urban planning. Incorporating green infrastructure and optimizing urban design could significantly mitigate HW impacts, particularly in densely urbanized areas like Milan. Meanwhile, cities like Lecce demonstrate the potential for urban planning strategies that take advantage of the existing environmental benefits, such as proximity to cooling coastal influences, to further enhance resilience. Such integrated approaches are essential for addressing the intensifying challenges of extreme heat events in urban areas.

5. Conclusions

In recent decades, episodes of high air temperature and heat waves have become more persistent in different areas of planet Earth. In the future, these exceptional situations will affect more and more areas, exacerbating their social, economic, and environmental impact. A better understanding of these conditions is needed to establish resilience measures that can improve the climate conditions in cities. In this regard, the use of the actual morphological characterization of cities, instead of the LCZ classification, has made it possible to identify the critical role of parameters such as building height, aspect ratio, sky view factor, and surface coverage in modelling the thermal characteristics of urban environments. The present work therefore analyzed the correlations between SUHII and actual urban morphological parameters in Milan and Lecce, offering insights into urban vulnerability to extreme weather events such as heat waves.

The analysis of the relationship between SUHII and morphological parameters showed strong results, with R^2 values almost always above 0.9. These findings could be valuable for developing statistical models (e.g., machine learning) and could serve as useful tools

for identifying areas most affected by extreme events. Additionally, they could support the implementation of mitigation strategies and guide urban planning or redevelopment projects. Multicollinearity and multiple linear regression analyses revealed that the main drivers influencing SUHII in both cities are ISF and HM. The contrasting impacts observed highlight that the influence of urban morphological factors varies significantly depending on site-specific characteristics. SUHII in cities increase during heat waves. The average increase is about 1 °C and is greater during nighttime than during the daytime. Inland cities, such as Milan, experience the largest increase in LST during the night, while cities near the sea, such as Lecce, experience a smaller increase. Lecce also shows a negative SUHII during the day, which is amplified during the heat wave. This dynamic is strongly associated with the behavior of the soil moisture in the surrounding rural area which could show values typical of desert and arid areas. This may underline how this phenomenon is not only relegated to arid-desert areas but is also present in some Mediterranean cities.

By understanding the morphological characteristics associated with increased thermal anomalies, urban planners can prioritize mitigation efforts, such as increasing green spaces or implementing cool roofing technologies, in vulnerable areas. To mitigate SUHII effects, it is crucial to incorporate urban morphology considerations into climate adaptation strategies. Milan would benefit from increasing vegetation cover, implementing green roofs, urban forests, and using reflective building materials. Conversely, Lecce's approach, with its low-rise buildings and abundant green areas, serves as an exemplary model for other cities aiming to reduce urban heat stress. These findings emphasize the need to consider spatial and temporal variability in assessing the impact of urban morphology on heat island intensity, as well as the thermal properties of urban surfaces, which are increasingly available in global datasets. Future research should explore additional urban variables to better understand their influence on thermal patterns, helping to develop more targeted strategies for reducing SUHII. Long-term effects of climate change and the effectiveness of mitigation strategies should also be studied. Expanding research to cities with diverse climates and urban layouts will provide a broader understanding of SUHII, benefiting global urban planning. Future studies should focus on the relationship between SUHII and wind patterns, using reanalysis data like ERA5 for deeper insights. In addition, it is worth extending the study of relationships by also considering the thermal properties of urban surfaces (such as albedo) and the presence of vegetation, through vegetation indices (i.e., the leaf area index).

In conclusion, this research underscores the critical role of urban morphology in shaping SUHII effects and the necessity of tailored urban planning interventions to enhance urban resilience.

Author Contributions: Conceptualization, A.E., G.P. and R.B.; methodology, G.P. and R.B.; software, A.E.; validation, A.E.; formal analysis, A.E. and G.P.; investigation, A.E.; resources, R.B.; data curation, G.P.; writing—original draft preparation, A.E.; writing—review and editing, G.P., A.D., G.M., P.S., T.S., J.L.S. and R.B.; visualization, A.E.; supervision, G.P. and R.B.; project administration, R.B.; funding acquisition, R.B. All authors have read and agreed to the published version of the manuscript.

Funding: A.E. acknowledges the PhD financial support of the Italian Ministry of University and Research (MUR) by the PON "Ricerca e Innovazione 2014–2020—Asse IV"—PhD course in "Scienze e Tecnologie Biologiche ed Ambientali"–XXXVII cycle-University of Salento.

Data Availability Statement: Derived data supporting the findings of this study are available from the corresponding author on request.

Acknowledgments: The authors thank Enzo Papandrea for his assistance with the code for downloading Sentinel data and Fabio Bozzeda for his help with the statistical analysis. T.S. acknowledges the Project IR0000032—ITINERIS—Italian Integrated Environmental Research Infrastructures System—CUP B53C22002150006EU funded by Next Generation EU Mission 4 "Education and Research"—Component 2: "From research to business"—Investment 3.1: "Fund for the realisation of an integrated system of research and innovation infrastructures" (views and opinions expressed are however those of the authors only and do not necessarily reflect those of the European

Union or the European Commission. Neither the European Union nor European Commission can be held responsible for them).

Conflicts of Interest: Author Giuseppe Maffeis was employed by the company TerrAria s.r.l. The remaining authors declare that the research was conducted in the absence of any commercial or financial relationships that could be construed as a potential conflict of interest.

References

1. Oke, T.; Mills, G.; Christen, A.; Voogt, J. *Urban Climates*; Cambridge University Press: Cambridge, UK, 2017.
2. Santamouris, M. *Energy and Climate in the Urban Built Environment*; Routledge: London, UK, 2014; ISBN 978-0419221306.
3. Li, Y.; Schubert, S.; Kropp, J.P.; Rybski, D. On the influence of density and morphology on the Urban Heat Island intensity. *Nat. Commun.* **2020**, *11*, 2647. [CrossRef] [PubMed]
4. Oke, T.R. The urban energy balance. *Prog. Phys. Geogr. Earth Environ.* **1988**, *12*, 471–508. [CrossRef]
5. Sailor, D.J. A review of methods for estimating anthropogenic heat and moisture emissions in the urban environment. *Int. J. Climatol.* **2011**, *31*, 189–199. [CrossRef]
6. Weng, Q. Thermal infrared remote sensing for urban climate and environmental studies: Methods, applications, and trends. *ISPRS J. Photogramm. Remote Sens.* **2009**, *64*, 335–344. [CrossRef]
7. Agathangelidis, I.; Cartalis, C.; Santamouris, M. Urban Morphological Controls on Surface Thermal Dynamics: A Comparative Assessment of Major European Cities with a Focus on Athens, Greece. *Climate* **2020**, *8*, 131. [CrossRef]
8. Berger, C.; Rosentreter, J.; Voltersen, M.; Baumgart, C.; Schmullius, C.; Hese, S. Spatio-temporal analysis of the relationship between 2D/3D urban site characteristics and land surface temperature. *Remote Sens. Environ.* **2017**, *193*, 225–243. [CrossRef]
9. Chun, B.; Guhathakurta, S. Daytime and nighttime urban heat islands statistical models for Atlanta. *Environ. Plan. B Urban Anal. City Sci.* **2017**, *44*, 308–327. [CrossRef]
10. Cai, Z.; Han, G.; Chen, M. Do water bodies play an important role in the relationship between urban form and land surface temperature? *Sustain. Cities Soc.* **2018**, *39*, 487–498. [CrossRef]
11. Zheng, Z.; Zhou, W.; Yan, J.; Qian, Y.; Wang, J.; Li, W. The higher, the cooler? Effects of building height on land surface temperatures in residential areas of Beijing. *Phys. Chem. Earth Parts A/B/C* **2019**, *110*, 149–156. [CrossRef]
12. Li, Z.; Hu, D. Exploring the relationship between the 2D/3D architectural morphology and urban land surface temperature based on a boosted regression tree: A case study of Beijing, China. *Sustain. Cities Soc.* **2022**, *78*, 103392. [CrossRef]
13. Zeng, P.; Sun, F.; Liu, Y.; Tian, T.; Wu, J.; Dong, Q.; Peng, S.; Che, Y. The influence of the landscape pattern on the urban land surface temperature varies with the ratio of land components: Insights from 2D/3D building/vegetation metrics. *Sustain. Cities Soc.* **2022**, *78*, 103599. [CrossRef]
14. Zhang, Y.; Chen, L.; Wang, Y.; Chen, L.; Yao, F.; Wu, P.; Wang, B.; Li, Y.; Zhou, T.; Zhang, T. Research on the Contribution of Urban Land Surface Moisture to the Alleviation Effect of Urban Land Surface Heat Based on Landsat 8 Data. *Remote Sens.* **2015**, *7*, 10737–10762. [CrossRef]
15. Imhoff, M.L.; Zhang, P.; Wolfe, R.E.; Bounoua, L. Remote sensing of the urban heat island effect across biomes in the continental USA. *Remote Sens. Environ.* **2010**, *114*, 504–513. [CrossRef]
16. Li, J.; Song, C.; Cao, L.; Zhu, F.; Meng, X.; Wu, J. Impacts of landscape structure on surface urban heat islands: A case study of Shanghai, China. *Remote Sens. Environ.* **2011**, *115*, 3249–3263. [CrossRef]
17. Rasul, A.; Balzter, H.; Smith, C. Spatial variation of the daytime surface urban cool island during the dry season in Erbil, Iraqi Kurdistan, from Landsat 8. *Urban Clim.* **2015**, *14*, 176–186. [CrossRef]
18. Azmi, R.; Koumetio, C.S.T.; Diop, E.B.; Chenal, J. Exploring the relationship between urban form and land surface temperature (LST) in a semi-arid region case study of Ben Guerir city—Morocco. *Environ. Chall.* **2021**, *5*, 100229. [CrossRef]
19. Hidalgo García, D.; Arco Díaz, J. Modeling of the Urban Heat Island on local climatic zones of a city using Sentinel 3 images: Urban determining factors. *Urban Clim.* **2021**, *37*, 100840. [CrossRef]
20. Delgado-Capel, M.J.; Cariñanos, P.; Escudero-Viñolo, M. Capacity of Urban Green Infrastructure Spaces to Ameliorate Heat Wave Impacts in Mediterranean Compact Cities: Case Study of Granada (South-Eastern Spain). *Land* **2023**, *12*, 1076. [CrossRef]
21. Hidalgo García, D.; Arco Díaz, J.; Martín Martín, A.; Gómez Cobos, E. Spatiotemporal Analysis of Urban Thermal Effects Caused by Heat Waves through Remote Sensing. *Sustainability* **2022**, *14*, 12262. [CrossRef]
22. An, N.; Dou, J.; González-Cruz, J.E.; Bornstein, R.D.; Miao, S.; Li, L. An observational case study of synergies between an intense heat wave and the urban heat island in Beijing. *J. Appl. Meteorol. Climatol.* **2020**, *59*, 605–620. [CrossRef]
23. Jiang, S.; Lee, X.; Wang, J.; Wang, K. Amplified Urban Heat Islands during Heat Wave Periods. *J. Geophys. Res. Atmos.* **2019**, *124*, 7797–7812. [CrossRef]
24. Joshi, K.; Khan, A.; Anand, P.; Sen, J. Understanding the synergy between heat waves and the built environment: A three-decade systematic review informing policies for mitigating urban heat island in cities. *Sustain. Earth Rev.* **2024**, *7*, 25. [CrossRef]
25. Diem, P.K.; Nguyen, C.T.; Diem, N.K.; Diep, N.T.; Thao, P.T.; Hong, T.G.; Phan, T.N. Remote sensing for urban heat island research: Progress, current issues, and perspectives. *Remote Sens. Appl. Soc. Environ.* **2024**, *33*, 101081. [CrossRef]

26. Du, H.; Zhan, W.; Liu, Z.; Krayenhoff, E.S.; Chakraborty, T.C.; Zhao, L.; Jiang, L.; Dong, P.; Li, L.; Huang, F.; et al. Global mapping of urban thermal anisotropy reveals substantial potential biases for remotely sensed urban climates. *Sci. Bull.* **2023**, *68*, 1809–1818. [CrossRef]
27. Esposito, A.; Grulois, M.; Pappaccogli, G.; Palusci, O.; Donateo, A.; Salizzoni, P.; Santiago, J.L.; Martilli, A.; Maffeis, G.; Buccolieri, R. On the Calculation of Urban Morphological Parameters Using GIS: An Application to Italian Cities. *Atmosphere* **2023**, *14*, 329. [CrossRef]
28. Lindberg, F.; Grimmond, C.S.B. Continuous sky view factor maps from high resolution urban digital elevation models. *Clim. Res.* **2010**, *42*, 177–183. [CrossRef]
29. Bernard, J.; Bocher, E.; Petit, G.; Palominos, S. Sky View Factor Calculation in Urban Context: Computational Performance and Accuracy Analysis of Two Open and Free GIS Tools. *Climate* **2018**, *6*, 60. [CrossRef]
30. Dunn, R.J.; Alexander, L.V.; Donat, M.G.; Zhang, X.; Bador, M.; Herold, N.; Lippmann, T.; Allan, R.; Aguilar, E.; Barry, A.A.; et al. Development of an updated global land in situ-based data set of temperature and precipitation extremes: HadEX3. *J. Geophys. Res. Atmos.* **2020**, *125*, e2019JD032263. [CrossRef]
31. Donateo, A.; Palusci, O.; Pappaccogli, G.; Esposito, A.; Martilli, A.; Santiago, J.L.; Buccolieri, R. Analysis of urban heat island and human thermal comfort in a Mediterranean city: A case study of Lecce (Italy). *Sustain. Cities Soc.* **2023**, *98*, 104849. [CrossRef]
32. Barriopedro, D.; García-Herrera, R.; Ordóñez, C.; Miralles, D.G.; Salcedo-Sanz, S. Heat waves: Physical understanding and scientific challenges. *Rev. Geophys.* **2023**, *61*, e2022RG000780. [CrossRef]
33. Pappaccogli, G.; Giangrande, F.; Esposito, A.; Donateo, A.; Lionello, P.; Buccolieri, R. Dynamics of urban heat island intensity in Lecce, Italy: Seasonal, diurnal and heat wave influence. *Bull. Atmos. Sci. Technol.* **2024**, *5*, 8. [CrossRef]
34. Delle Rose, M.; Martano, P. Datasets of Groundwater Level and Surface Water Budget in a Central Mediterranean Site (21 June 2017–1 October 2022). *Data* **2023**, *8*, 38. [CrossRef]
35. Kutner, M.H.; Nachtsheim, C.J.; Neter, J. *Applied Linear Regression Models*, 4th ed.; McGraw-Hill/Irwin: New York, NY, USA, 2024.
36. Xu, X.; Wu, Y.; Lin, G.; Gong, J.; Chen, K. Exploring diurnal and seasonal variabilities in surface urban heat island intensity in the Guangdong-Hong Kong-Macao Greater Bay Area. *J. Geogr. Sci.* **2024**, *34*, 1472–1492. [CrossRef]
37. Ma, L.; Wang, Y.; Liang, Z.; Ding, J.; Shen, J.; Wei, F.; Li, S. Changing Effect of Urban Form on the Seasonal and Diurnal Variations of Surface Urban Heat Island Intensities (SUHIIs) in More Than 3000 Cities in China. *Sustainability* **2021**, *13*, 2877. [CrossRef]
38. Stathopoulou, M.; Constantinos, C. Study of the urban heat island of Athens, Greece during daytime and night-time. In Proceedings of the 2007 Urban Remote Sensing Joint Event, Paris, France, 11–13 April 2007.
39. Hartz, D.A.; Prashad, L.; Hedquist, B.C.; Golden, J.; Brazel, A.J. Linking satellite images and hand-held infrared thermography to observed neighborhood climate conditions. *Remote Sens. Environ.* **2006**, *104*, 190–200. [CrossRef]
40. Rajeswari, J.R.; Fountoukis, C.; Siddique, A.; Moosakutty, S.; Mohieldeen, Y.; Ayoub, M.A.; Alfarra, M.R. Urban heat island phenomenon in a desert, coastal city: The impact of urbanization. *Urban Clim.* **2024**, *56*, 102016. [CrossRef]
41. Jiang, K.; Pan, Z.; Pan, F.; Teuling, A.J.; Han, G.; An, P.; Chen, X.; Wang, J.; Song, Y.; Cheng, L.; et al. Combined influence of soil moisture and atmospheric humidity on land surface temperature under different climatic background. *iScience* **2023**, *26*, 106837. [CrossRef]
42. Guarino, M.V.; Martilli, A.; Di Sabatino, S.D.; Leo, L.S. *Modelling The Urban Boundary-Layer over a Typical Mediterranean City Using Wrf: Assessment of Uhi And Thermal Comfort*; American Society of Mechanical Engineers: New York, NY, USA, 2004; pp. 304–307.
43. Johansson, E. Influence of urban geometry on outdoor thermal comfort in a hot dry climate: A study in Fez, Morocco. *Build. Environ.* **2006**, *41*, 1326–1338. [CrossRef]
44. Touchaei, A.G.; Akbari, H. Evaluation of the seasonal effect of increasing the albedo on urban climate and energy consumption of buildings in Montreal. *Urban Clim.* **2015**, *14*, 278–289. [CrossRef]
45. Touchaei, A.G.; Hosseini, M.; Akbari, H. Energy savings potentials of commercial buildings by urban heat island reduction strategies in Montreal (Canada). *Energy Build.* **2016**, *110*, 41–48. [CrossRef]
46. Touchaei, A.G.; Wang, Y. Characterizing urban heat island in Montreal (Canada)—Effect of urban morphology. *Sustain. Cities Soc.* **2015**, *19*, 395–402. [CrossRef]